An investigation of one- versus two-dimensional semiclassical transition state theory for H atom abstraction and exchange reactions

Samuel M. Greene, Xiao Shan, and David C. Clary

Citation: The Journal of Chemical Physics **144**, 084113 (2016);
View online: https://doi.org/10.1063/1.4942161
View Table of Contents: http://aip.scitation.org/toc/jcp/144/8
Published by the American Institute of Physics

An investigation of one- versus two-dimensional semiclassical transition state theory for H atom abstraction and exchange reactions

Samuel M. Greene,[a] Xiao Shan, and David C. Clary
Physical and Theoretical Chemistry Laboratory, Department of Chemistry, University of Oxford, South Parks Road, Oxford OX1 3QZ, United Kingdom

(Received 14 December 2015; accepted 1 February 2016; published online 25 February 2016)

We investigate which terms in Reduced-Dimensionality Semiclassical Transition State Theory (RD SCTST) contribute most significantly in rate constant calculations of hydrogen extraction and exchange reactions of hydrocarbons. We also investigate the importance of deep tunneling corrections to the theory. In addition, we introduce a novel formulation of the theory in Jacobi coordinates. For the reactions of H atoms with methane, ethane, and cyclopropane, we find that a one-dimensional (1-D) version of the theory without deep tunneling corrections compares well with 2-D SCTST results and accurate quantum scattering results. For the "heavy-light-heavy" H atom exchange reaction between CH_3 and CH_4, deep tunneling corrections are needed to yield 1-D results that compare well with 2-D results. The finding that accurate rate constants can be obtained from derivatives of the potential along only one dimension further validates RD SCTST as a computationally efficient yet accurate rate constant theory. © *2016 AIP Publishing LLC.* [http://dx.doi.org/10.1063/1.4942161]

I. INTRODUCTION

Conventional quantum mechanical approaches to calculating reaction rate constants involve constructing a potential energy surface (PES) and performing either time-dependent or time-independent quantum reactive scattering (QRS) calculations on this PES.[1–6] However, these methods are usually limited to relatively small polyatomic systems due to the computational expense required to construct a PES and to perform QRS calculations.[4,7–9] The expense of constructing a PES scales roughly exponentially with the size of the system, and this is often the primary obstacle to performing QRS calculations for reactions involving more than four or five atoms.[10] The largest systems to which QRS has been applied are the $H + CH_4 \longrightarrow H_2 + CH_3$ and $H_2 + CH_3 \longrightarrow H + CH_4$ reactions.[11–19] QRS results from different PESs exhibited good agreement with each other and with experimental results.[20,21]

An alternative approach, variational transition state theory with multidimensional tunneling contributions (VTST/MT), is a class of efficient methods for rate constant calculations based on conventional transition state theory (TST). Tunneling effects on the rate constant are incorporated semiclassically through a one-dimensional (1-D) WKB integral.[22–24] Of these methods, VTST/LAG is the most accurate but also the most computationally expensive. The VTST/microcanonically optimized multidimensional tunneling (μOMT) method is a hybrid of VTST/small curvature tunneling (SCT) and VTST/LCG4 and yields results of similar accuracy with considerably less computational expense.[25] VTST/MT methods have been applied to a variety of reactions and generally yield results in good agreement to those from QRS and experiment.[25–33]

Additionally, Craig and Manolopoulos[34,35] adapted the Ring Polymer Molecular Dynamics (RPMD) method to rate constant calculations. This theory relies upon the isomorphism between a classical treatment of an infinite number of copies of the system coupled via harmonic potentials and a quantum mechanical treatment of a single copy of the system. Their method has yielded results in agreement with those from other methods.[26,27,30,36,37] Other theories include centroid molecular dynamics and related quantum mechanical formulations of TST.[38–41] Recently, Althorpe and Hele[42,43] showed that their formulation of quantum TST is identical to RPMD TST. Most of these more approximate methods require a complete PES and are thus faster than QRS methods only because of efficiency gains in kinetics calculations and not because of a reduced need for PES calculations.

Semiclassical Transition State Theory (SCTST), developed by Miller *et al.*,[44–46] depends only on derivatives of the PES at the transition state and the reaction barrier height, thereby potentially reducing the number of PES calculations required. Effectively, a one-dimensional potential barrier along the reaction coordinate is extrapolated from derivatives of the PES, and coupling among degrees of freedom (DOFs) is included in the barrier's shape. The probability of tunneling through the barrier is calculated using WKB Theory.[47] SCTST in its original form is derived from second-order vibrational perturbation theory (VPT2) applied to a fourth-order Taylor expansion of the potential at the transition state,[48] and it therefore relies on the harmonic frequencies and anharmonic constants of the transition state.[49–52] It can also be adapted for higher-order approaches.[53] Exact SCTST kinetics calculations are often computationally intractable for reactions involving more than three or four atoms, but more efficient approximations (Multidimensional Monte Carlo Integration and the Wang-Landau Algorithm) have been developed and shown to yield accurate results.[54]

[a]Electronic mail: samuel.greene@chem.ox.ac.uk

SCTST has been applied previously to several reactions with considerable success.[55–59] However, as it depends on the presence of a transition state, it may not be applicable to barrierless reactions or reactions with low barriers. Recently, Wagner[60] developed an alternative method for constructing the potential barrier used in SCTST, in which additional constraints are applied such that the reactant and product asymptotes are more physically realistic. This method thereby enables more accurate calculation of tunneling probabilities, particularly at low energies ("deep tunneling"), at minimal additional computational expense.

In the past decade, reduced-dimensionality (RD) approaches to QRS have enabled rate constant calculations for reactions involving more than six atoms.[5,10,61–67] In RD methods, only a subset of the system's DOFs are treated explicitly, while the remaining DOFs are treated by more approximate methods. The primary computational advantage of this approach lies in the significant reduction of the number of *ab initio* calculations required to construct an RD PES, although RD kinetics calculations are generally also less computationally expensive than their full-dimensional (FD) counterparts. Several different approaches to choosing which DOFs to treat explicitly have been tested and discussed previously.[19,68–75] Recent work in our group has involved treating explicitly only the DOFs corresponding to the bonds being formed or broken in RD QRS calculations.[76–78] This has enabled the application of QRS to reactions involving molecules as large as butane,[79] generally with results that agree with experiment and theory at a fraction of the expense of FD QRS calculations.

Recently, we developed Reduced-Dimensionality Semi-classical Transition State Theory (RD SCTST) as a potential method for further improving the efficiency of rate constant calculations.[80] In RD SCTST, anharmonic constants are calculated for only a subset of DOFs, and the remaining DOFs are treated harmonically. We applied RD SCTST to three gas-phase H atom abstraction and exchange reactions for which 2-D PESs had been developed previously.[77,78] The resulting rate constants exhibited excellent agreement with RD QRS rate constants calculated previously using these PESs. Notably, agreement was observed for the reaction $CH_3 + CH_4 \longrightarrow CH_4 + CH_3$, which has large reaction-path curvature. "Corner-cutting" effects along paths in the concave region of the PES between the reactant and product channels have been shown to contribute significantly to rate constants for reactions of this type.[81–84] RD SCTST results agreed with QRS results even though this region of the PES is not considered in RD SCTST.

In a 2-D SCTST calculation, anharmonic constants are calculated for two vibrational DOFs: the reaction mode, which has an associated imaginary frequency, and the transition mode, which is orthogonal to the reaction mode and has a real frequency. 2-D SCTST can be considered to account for the anharmonicity of each of these modes and the coupling between them. In this study, we seek to understand the extent to which the anharmonicity of the transition mode and the coupling between the modes contributes to rate constants calculated using 2-D SCTST. In particular, we perform 1-D SCTST calculations that account only for the anharmonicity of the reaction mode and compare their results to those from 2-D calculations. We previously investigated the effect of the deep tunneling corrections to SCTST within the 2-D framework,[80] and we here investigate their effect in 1-D. We consider four reactions, three of which were considered in our previous study, and for all of which 2-D PESs have been constructed previously,[76–78]

$$H + CH_4 \longrightarrow H_2 + CH_3, \quad (1)$$

$$H + C_2H_6 \longrightarrow H_2 + C_2H_5, \quad (2)$$

$$H + \text{cyc-}C_3H_6 \longrightarrow H_2 + \text{cyc-}C_3H_5, \quad (3)$$

$$CH_3 + CH_4 \longrightarrow CH_4 + CH_3. \quad (4)$$

These prototypical reactions serve as baseline tests of rate constant theories. Reactions (1)–(3) have significance in combustion processes.[76,78,85] All reactions involve the abstraction or exchange of a light H atom, indicating that quantum mechanical effects contribute significantly to the reaction rate, particularly at low temperatures. A comparison with results from TST allows for evaluation of the accuracy with which different methods recover these effects. In this study, we use previous QRS results as a basis of comparison because they were calculated using the same 2-D PESs. We seek only to evaluate RD SCTST as a method for kinetics calculations and not to evaluate the validity of the PESs considered.

The remainder of this paper is organized as follows. In Section II, formulas for 2-D and 1-D SCTST calculations are presented, as well as a novel method for calculating frequencies and anharmonic constants in Jacobi coordinates. In Section III, we present rate constants calculated using 2-D and 1-D SCTST and investigate the factors that contribute to differences between results from both methods. Section IV summarizes the key findings of this study.

II. METHODS

A. Reduced-dimensionality potential energy surface construction

Methods for the construction of the reduced-dimensionality potential energy surfaces (RD PESs) considered in this study are presented in previous studies.[76–78] Briefly, *ab initio* calculations are performed on a grid in (r_1, r_2) coordinate space. For the generic hydrogen atom abstraction or exchange reaction $Y + H_aZ \longrightarrow YH_a + Z$, r_1 is the Y-H_a distance, and r_2 is the distance between H_a and the atom in Z to which H_a is bonded (Fig. 1). At each grid point, the $3N - 8$ degrees of freedom other than r_1 and r_2 (the "spectator modes") are optimized, and the energy is then calculated at a high level of theory. The zero-point energy (ZPE) of the spectator modes is then added to this energy.

At each grid point, the Jacobi coordinates r and R are calculated from the optimized geometry. r is defined as the distance between H_a and the Y atom or moiety (H for reactions (1)–(3), and the C atom in CH_3 for reaction (4)). For reactions (1) and (4), R is the distance between the centers of mass of fragments YH_a and Z. For reactions (2) and (3), R is defined differently as the distance between the center of mass of YH_a and the atom in the Z fragment to which H_a is bonded. In

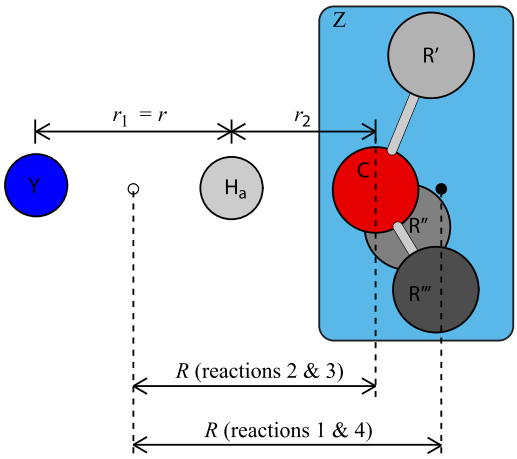

FIG. 1. The bond lengths (r_1 and r_2) and Jacobi coordinates (r and R) used to construct the PESs for the generic reaction $Y + H_aZ \longrightarrow YH_a + Z$. The Z fragment represents a hydrocarbon, with R′, R″, and R‴ bonded to the central C atom. The white and black circles denote the centers of mass of H_aY and Z, respectively. Note the differing definitions of the Jacobi coordinate R among the reactions considered in this study.

the case of reaction (3), this choice was made due to the presence of a van der Waals complex that affects the behavior of the minimum-energy path (MEP) in conventional Jacobi coordinates. This has been discussed in more detail previously.[78] Both definitions of R are consistent with the Bending-Corrected Rotating Linear Model[62] used in QRS calculations and with the treatment of the system as a three-body system in this study, as it is equally valid to consider the motion of Y and H_a relative to either the center of mass of Z or the C atom in Z.

Jacobi coordinates were then transformed into hyperspherical coordinates ρ and δ as follows:

$$\rho = \left[\left(\frac{m_1}{\mu}\right)R^2 + \left(\frac{m_2}{\mu}\right)r^2\right]^{1/2}, \tag{5a}$$

$$\delta = \tan^{-1}\left[\frac{r}{R}\left(\frac{m_2}{m_1}\right)^{1/2}\right], \tag{5b}$$

where

$$m_1 = \frac{(m_Y + m_H)m_Z}{m_Y + m_H + m_Z} \tag{6}$$

and

$$m_2 = \frac{m_Y m_H}{m_Y + m_H}, \tag{7}$$

where m_Y and m_Z are the masses of the Y and Z fragments, respectively, and m_H is the mass of an H atom. Although the mass μ uniquely defines a transformation from Jacobi to hyperspherical coordinates, it can be defined arbitrarily for the purpose of QRS calculations due to the presence of a factor of μ in the Hamiltonian operator expressed in hyperspherical coordinates. μ was defined differently among the PESs considered in this study. Following this coordinate transformation to hyperspherical coordinates, the ZPE-corrected *ab initio* energies were then fit to a double-Morse potential function, $V(\rho,\delta)$, in hyperspherical coordinates. Detailed discussions of the choice of this function and the fitting procedures can be found in previous studies and references within.[78,86]

B. Two-dimensional semiclassical transition state theory

1. Theoretical overview

Detailed discussions of SCTST and its derivation can be found elsewhere.[44–46,55,58] The modifications to SCTST required to use it within a reduced-dimensionality (RD) framework are described in Ref. 80. In an RD SCTST calculation, the set of F internal degrees of freedom of the transition state is partitioned into two sets of d active modes and $F - d$ spectator modes. One active mode, the reaction mode, has an imaginary frequency and is associated with motion along the reaction coordinate. The remaining $d - 1$ active modes are referred to as transition modes, have real frequencies, and are orthogonal to the reaction mode. Anharmonic constants for the active modes are included in the calculation of the rate constant, and the spectator modes are treated harmonically.

2. Anharmonic constants

In a two-dimensional calculation, there is one transition mode and therefore three unique anharmonic constants: one diagonal anharmonic constant for the reaction mode (x_{FF}), one diagonal anharmonic constant for the transition mode (x_{11}), and one off-diagonal anharmonic constant (x_{1F}). Formulas for these anharmonic constants are as follows:[46]

$$x_{FF} = \frac{\hbar^2}{16\omega_F^2}\left(f_{FFFF} - \frac{5f_{FFF}^2}{3\omega_F^2} - \frac{f_{1FF}^2(8\omega_F^2 - 3\omega_1^2)}{\omega_1^2(4\omega_F^2 - \omega_1^2)}\right), \tag{8a}$$

$$x_{11} = \frac{\hbar^2}{16\omega_1^2}\left(f_{1111} - \frac{5f_{111}^2}{3\omega_1^2} - \frac{f_{11F}^2(8\omega_1^2 - 3\omega_F^2)}{\omega_F^2(4\omega_1^2 - \omega_F^2)}\right), \tag{8b}$$

$$x_{1F} = \frac{\hbar^2}{4\omega_1\omega_F}\left(f_{11FF} - \frac{f_{111}f_{1FF}}{\omega_1^2} - \frac{f_{11F}f_{FFF}}{\omega_F^2} + \frac{2f_{11F}^2\omega_F^2}{[(\omega_1 + \omega_F)^2 - \omega_1^2][(\omega_1 - \omega_F)^2 - \omega_1^2]} + \frac{2f_{1FF}^2\omega_1^2}{[(\omega_1 + \omega_F)^2 - \omega_F^2][(\omega_1 - \omega_F)^2 - \omega_F^2]}\right), \tag{8c}$$

where ω_1 and ω_F are the harmonic frequencies for the transition and reaction modes, respectively, and the f terms denote third and fourth derivatives of the potential with respect to normal mode eigenvectors. In an RD calculation, the spectator modes are assumed not to contribute to the anharmonic constants for the active modes. The frequencies and normal mode eigenvectors of the active modes are obtained from a harmonic analysis of the transition state. Details of these calculations will be discussed below.

In a one-dimensional rate constant calculation, third and fourth derivatives with respect to the transition mode (f_{111}, f_{11F}, f_{1FF}, f_{1111}, and f_{11FF}) are considered to be 0, such that the transition mode is treated harmonically as a spectator mode. Within this framework, x_{11} and x_{1F} are 0, and x_{FF} is calculated as follows:

$$x_{FF} = \frac{\hbar^2}{16\omega_F^2}\left(f_{FFFF} - \frac{5f_{FFF}^2}{3\omega_F^2}\right). \tag{9}$$

It is interesting to note that the 2-D and 1-D diagonal anharmonic constants for the reaction mode (x_{FF}) differ because the 2-D constant depends on f_{1FF}.

3. Frequency and anharmonic constant calculations in Jacobi coordinates

In this study, the active modes are linear combinations of the Jacobi coordinates. Here we present a method for calculating the frequencies and anharmonic constants for these modes. Previously,[80] we transformed the Jacobi coordinates to the Cartesian coordinates of the Y, H_a, and Z fragments along one dimension, assuming a collinear geometry. Using Jacobi coordinates removes the need for this assumption.

The transition state is modeled as a system of three particles with masses m_Y, m_H, and m_Z and velocities $\vec{v_Y}$, $\vec{v_H}$, and $\vec{v_Z}$. Subtracting the kinetic energy associated with center-of-mass translation of the system,

$$T_{COM} = \frac{1}{2}\left(m_Y + m_H + m_Z\right)\left(\frac{m_Y\vec{v_Y} + m_H\vec{v_H} + m_Z\vec{v_Z}}{m_Y + m_H + m_Z}\right)^2, \tag{10}$$

from the total kinetic energy of the system,

$$T_{tot} = \frac{1}{2}\left(m_Y\vec{v_Y}^2 + m_H\vec{v_H}^2 + m_Z\vec{v_Z}^2\right), \tag{11}$$

yields the following, after simplification:

$$T_{Jac} = \frac{1}{2}\left(m_1 v_R^2 + m_2 v_r^2\right), \tag{12}$$

where v_R and v_r are the time derivatives of the Jacobi coordinates, and m_1 and m_2 are defined as in Eqs. (6) and (7). Expanding the potential V as a Taylor series to second order in R and r enables a typical normal mode analysis, whereby the mass-weighted Hessian in Jacobi coordinates H is diagonalized to obtain two frequencies and normal mode eigenvectors,

$$H = \begin{pmatrix} m_1^{-1}\frac{\partial^2 V}{\partial^2 R} & (m_1 m_2)^{-1/2}\frac{\partial^2 V}{\partial R \partial r} \\ (m_1 m_2)^{-1/2}\frac{\partial^2 V}{\partial R \partial r} & m_2^{-1}\frac{\partial^2 V}{\partial^2 r} \end{pmatrix}. \tag{13}$$

Derivatives with respect to Jacobi coordinates are calculated from derivatives with respect to hyperspherical coordinates using the chain rule,

$$\frac{\partial}{\partial r} = \left(\frac{m_2}{\mu}\right)^{1/2}\left(\sin\delta\frac{\partial}{\partial\rho} + \frac{\cos\delta}{\rho}\frac{\partial}{\partial\delta}\right), \tag{14a}$$

$$\frac{\partial}{\partial R} = \left(\frac{m_1}{\mu}\right)^{1/2}\left(\cos\delta\frac{\partial}{\partial\rho} - \frac{\sin\delta}{\rho}\frac{\partial}{\partial\delta}\right), \tag{14b}$$

where μ is the mass used to construct the corresponding PES. Anharmonic constants are calculated from derivatives of the potential with respect to the normal mode eigenvectors $\vec{q}_1$ and $\vec{q}_2$,

$$\frac{\partial}{\partial\vec{q}_i} = \vec{q}_i \cdot \left(m_1^{-1/2}\frac{\partial}{\partial R}, m_2^{-1/2}\frac{\partial}{\partial r}\right). \tag{15}$$

In the present study, these derivatives were calculated analytically from the PESs using Mathematica version 8.0.[87] The frequencies and anharmonic constants calculated by this method were equivalent to those calculated previously from these PESs using Cartesian coordinates.[80] Calculating the third and fourth derivatives of the PES required for 2-D SCTST calculations analytically was, on average, 43 times faster in Jacobi coordinates than in Cartesian coordinates for the reactions considered in this study. Calculating the derivatives required for a 1-D calculation in Jacobi coordinates is, on average, 3.09 times faster than for a 2-D calculation.

4. Thermal rate constants

The rate constant $k(T)$ is calculated from the cumulative reaction probability (CRP), $N(E_v)$, as follows:[58]

$$k(T) = \frac{1}{h}\frac{Q^{\ddagger}_{trans}(T)Q^{\ddagger}_{rot}(T)Q^{\ddagger}_{elec}(T)Q^{\ddagger}_{spec}(T)\int_{E_{thresh}}^{\infty} N(E_v)\,\exp\left(-E_v k_B^{-1}T^{-1}\right)\mathrm{d}E_v}{Q_r(T)}, \tag{16}$$

where $Q_r(T)$ is the partition function for the reactants, and $Q^{\ddagger}_{trans}(T)$, $Q^{\ddagger}_{rot}(T)$, and $Q^{\ddagger}_{elec}(T)$ are the translational, rotational, and electronic partition functions for the transition state. $Q^{\ddagger}_{spec}(T)$ is a vibrational partition function for the spectator modes of the transition state. All rotational and vibrational partition functions were calculated from geometries and harmonic frequencies presented in the previous studies associated with these PESs.[76–78] As in these previous studies, the electronic partition functions of all closed- and open-shell species were considered to be 1 and 2, respectively, as the first excited states of the species considered in this study have energies too great to appreciably contribute. E_v represents the total energy in the active modes of the transition state. E_{thresh} is the least energy at which tunneling through the reaction barrier is possible.[80]

5. Semiclassical CRP

The CRP in 2-D SCTST is given as

$$N(E_v) = \sum_{n=0}^{n_{max}(E_v)} \left(1 + \exp(2\theta_n(E_v))\right)^{-1}, \tag{17}$$

where n_{max}, the maximum energetically allowed quantum number of the transition mode, is a function of E_v,[54]

$$n_{\max}(E_v) = \begin{cases} v_D & E_v \geq D \\ v_D\left(1 - \sqrt{1 - \frac{E_v}{D}}\right) & E_v < D \end{cases}, \quad (18)$$

with

$$v_D = -\frac{\hbar\omega_1}{2x_{11}} - \frac{1}{2} \quad (19)$$

and

$$D = -\frac{\hbar^2\omega_1^2}{4x_{11}}. \quad (20)$$

$\theta_n(E_v)$ represents the barrier penetration integral (cf. WKB Theory) associated with motion along the reaction coordinate. Note that this is a one-dimensional integral regardless of the number of active modes in the SCTST treatment. The influence of the transition mode on the barrier penetration integral is accounted for via its dependence on n, the quantum number of the transition mode. Miller *et al.*[46] give the following analytical formula for $\theta_n(E_v)$:

$$\theta_n(E_v) = \pi\frac{-\Omega_n + [\Omega_n^2 + 4x_{FF}(\Delta V_f^\ddagger - E_v + E_n)]^{1/2}}{2x_{FF}}, \quad (21)$$

where the subscript F denotes the reaction mode, and $\Delta V_f^\ddagger$ denotes the reaction's forward barrier height. E_n is the vibrational energy associated with the transition mode,

$$E_n = \hbar\omega_1\left(n + \frac{1}{2}\right) + x_{11}\left(n + \frac{1}{2}\right)^2. \quad (22)$$

Ω_n is calculated as follows:

$$\Omega_n = \mathrm{Im}\left[\hbar\omega_F + x_{1F}\left(n + \frac{1}{2}\right)\right]. \quad (23)$$

These formulas were rigorously derived from the VPT2 expression for the energy at the transition state.[45,46] This formula for $\theta_n(E_v)$ is equivalently the barrier penetration integral for a symmetric Eckart potential and for an inverted Morse potential appropriately fitted to $\Delta V_f^\ddagger$, x_{FF}, and Ω_n.[60,88] The functional form of this Eckart potential is as follows:

$$V_{se}(s) = \Delta V_f - D_{se} + 4D_{se}\frac{\exp(\alpha s)}{[1 + \exp(\alpha s)]^2}, \quad (24)$$

with

$$D_{se} = -\frac{\Omega_n^2}{4x_{FF}} \quad (25)$$

and

$$\alpha = \frac{(-8x_{FF})^{1/2}}{\hbar}, \quad (26)$$

where s represents the reaction coordinate, with units of (mass$^{1/2}$ length). This method for calculating the CRP and associated rate constants will be referred to as SCTST-M.

6. Semiclassical CRP with deep tunneling corrections

Wagner[60] noted that Eq. (21) sometimes inaccurately represents tunneling at energies near the reaction's quantum threshold energy. The reactant and product asymptotes of Eq. (24) are not E_{thresh}, as would be motivated by physical intuition, and are instead given as follows:

$$\lim_{s\to\pm\infty} V_{se}(s) = \Delta V_f^\ddagger - D_{se}. \quad (27)$$

Consequently, no tunneling occurs when $E_{\text{thresh}} < E_v < \Delta V_f^\ddagger - D_{se}$, which is physically unrealistic. To correct this, Wagner proposed that the barrier be modeled as a piecewise asymmetric Eckart potential. Details of the construction of this potential can be found in Ref. 60 and its supplementary material. It is defined such that its reactant asymptote is 0 and its product asymptote is $\Delta V_f^\ddagger - \Delta V_r^\ddagger$, where $\Delta V_r^\ddagger$ is the reaction's reverse barrier height, which ensures that tunneling is possible at all energies greater than E_{thresh}. The potential is also defined to be smooth and continuous. The barrier penetration integral for this potential can be calculated analytically to obtain $\theta_n(E_v)$.[60] $P_n(E_v)$ is calculated from $\theta_n(E_v)$ as described previously.[24,80] This method for calculating the CRP and rate constants will be referred to as SCTST-W.

7. Barrier height calculations

Forward and reverse barrier heights were calculated from points on the PES corresponding to the transition state (TS), product, and reactant geometries. The TS was considered to be the saddle point of the PES instead of the

TABLE I. Energetic parameters used in 1-D and 2-D SCTST calculations.[a]

	Reaction (1)		Reaction (2)		Reaction (3)		Reaction (4)	
	2-D	1-D	2-D	1-D	2-D	1-D	2-D	1-D
x_{FF} (cm^{-1})	−166.44	−248.68	−317.26	−485.39	−254.57	−539.89	−109.95	−174.01
x_{1F} (cm^{-1})	−160.59i	0	−340.96i	0	−618.85i	0	−32.78i	0
x_{11} (cm^{-1})	0.33	0	14.36	0	109.75	0	−1.64	0
G_0 (μE_h)	−240.43	−265.34	−383.86	−446.41	−338.20	−485.31	−195.75	−198.21
ω_F (cm^{-1})	1782.3i		1597.2i		1527.6i		1683.6i	
ω_1 (cm^{-1})	1352.9		1385.0		1537.5		494.7	
$\Delta V_f^\ddagger$ (kcal mol^{-1})	11.409		7.647		9.488		16.170	
$\Delta V_r^\ddagger$ (kcal mol^{-1})	11.786		4.504		4.800		16.170	

[a]Anharmonic constants (x_{FF}, x_{1F}, and x_{11}) are calculated according to Eqs. (8) and (9) and reported in cm^{-1}. The subscript F denotes the reaction mode, and the subscript 1 denotes the transition mode. The 1-D and 2-D G_0 parameters are calculated from Eqs. (29) and (30). The barrier heights used in SCTST calculations ($\Delta V_f^\ddagger$ and $\Delta V_r^\ddagger$) are reported in kcal mol^{-1}.

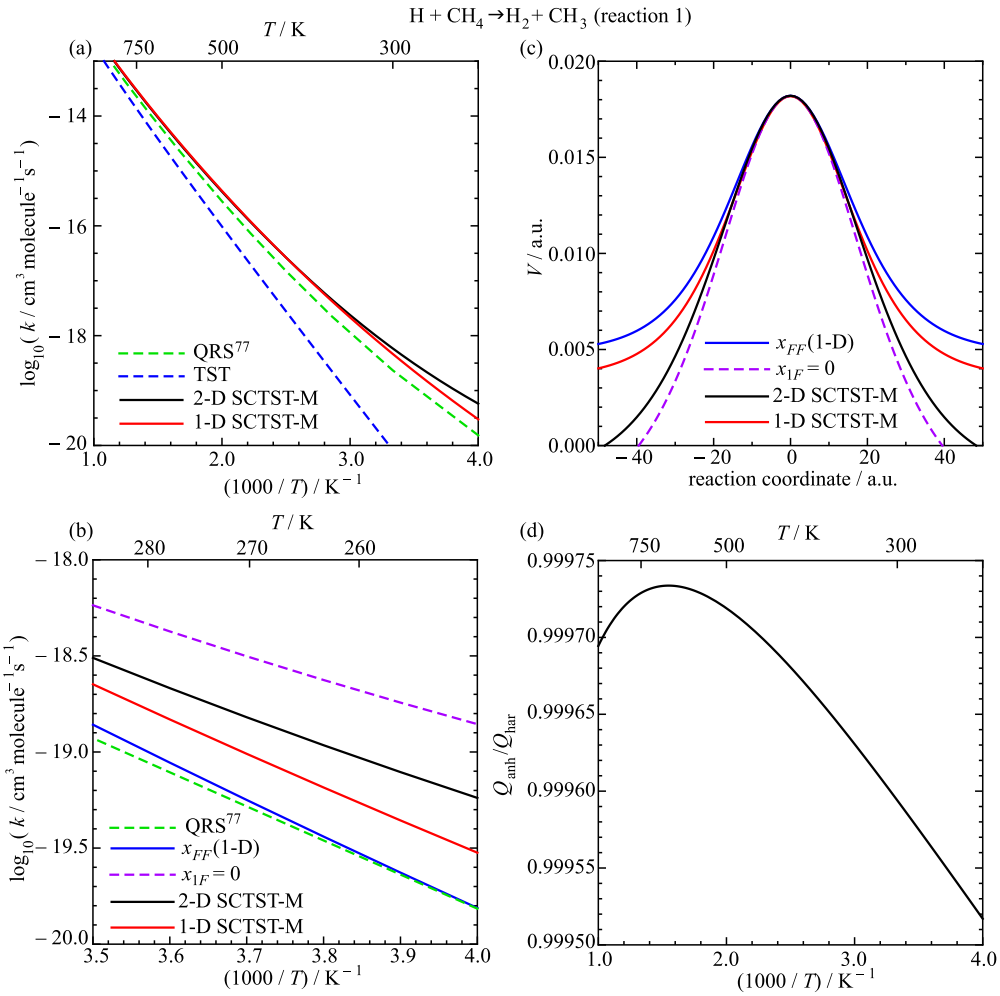

FIG. 2. (a) Rate constants calculated for reaction (1) as a function of temperature using TST (dashed red curve), the 2-D SCTST-M method (black curve), 1-D SCTST-M (blue curve), and QRS.[77] (b) Rate constants obtained by setting the parameters x_{1F} (magenta curve) and x_{FF} (orange curve) to their 1-D values, as given in Sec. II B 2. Note the different scale in this plot. (c) Symmetric Eckart potentials for $n = 0$ corresponding to the rate constant calculations presented in (b). (d) The ratio of the anharmonic to the harmonic partition functions for the transition mode as a function of temperature.

TS geometry calculated using *ab initio* methods and was found via numerical root-finding. The forward barrier height is calculated as follows:

$$\Delta V_f^{\ddagger} = V(\rho_{\rm TS}, \delta_{\rm TS}) - V(\rho_{\rm max}, \delta_r) + G_0 - \frac{\hbar}{2}\left(\frac{m_{\rm H}+m_{\rm Z}}{m_{\rm H}m_{\rm Z}}\frac{\partial^2 V}{\partial R^2}\Big|_{\rho=\rho_{\rm max},\delta=\delta_r}\right)^{1/2}, \quad (28)$$

where $(\rho_{\rm TS}, \delta_{\rm TS})$ is the TS geometry in hyperspherical coordinates, and $\rho_{\rm max}$ is the maximum value of ρ considered in QRS calculations performed on the PES. δ_r, the value of δ at the minimum of the reactant well at $\rho = \rho_{\rm max}$, was calculated numerically. The last term in Eq. (28) represents the zero-point energy of the vibration of the reactant C–H bond and must be included because zero-point energy is not included in the vibrational component of $Q_{\rm r}(T)$ (Eq. (16)). The zero-point energy of the TS is not included because it is included in E_n (Eq. (22)). G_0 arises from the calculation of the VPT2 energy and must be included in the barrier height for an SCTST calculation.[58] In the two-dimensional case, it is calculated as follows:[55]

$$G_0 = \sum_{i=1}^{2}\hbar^2\left(\frac{1}{64}\frac{f_{iiii}}{\omega_i^2} - \frac{5}{576}\frac{f_{iii}^2}{\omega_i^4}\right) + \frac{3}{64}\sum_{i\neq j}\frac{\hbar^2 f_{iij}^2}{\omega_i^2(4\omega_i^2-\omega_j^2)}. \quad (29)$$

Assuming that third and fourth derivatives involving the transition mode are 0 yields the following 1-D formula for G_0:

$$G_0 = \hbar^2\left(\frac{1}{64}\frac{f_{FFFF}}{\omega_F^2} - \frac{5}{576}\frac{f_{FFF}^2}{\omega_F^4}\right). \quad (30)$$

The reverse barrier height is calculated in a manner similar to the forward barrier height,

$$\Delta V_r^{\ddagger} = V(\rho_{\rm TS}, \delta_{\rm TS}) - V(\rho_{\rm max}, \delta_p) + G_0 - \frac{\hbar}{2}\left(\frac{m_{\rm H}+m_{\rm Y}}{m_{\rm H}m_{\rm Y}}\frac{\partial^2 V}{\partial r_1^2}\Big|_{\rho=\rho_{\rm max},\delta=\delta_p}\right)^{1/2}. \quad (31)$$

The derivative with respect to r_1, the product bond length, is approximated as follows, based on the assumption that the TS is collinear:

$$\frac{\partial}{\partial r_1} = \frac{\partial}{\partial r} + \frac{m_{\rm Y}}{m_{\rm Y}+m_{\rm H}}\frac{\partial}{\partial R}. \quad (32)$$

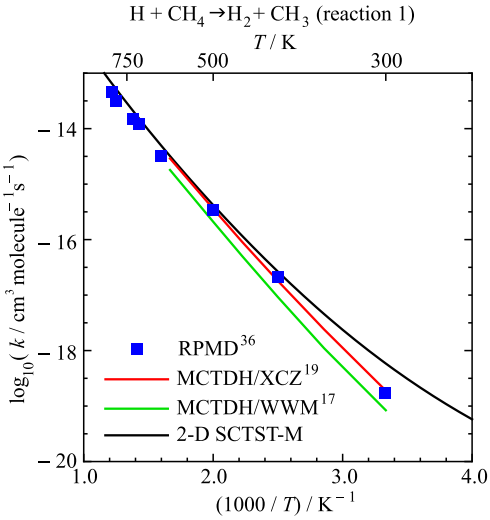

FIG. 3. Rate constants for reaction (1) from the 2-D SCTST-M method in this study (black curve) and from other theoretical studies. Results from RPMD[36] are presented as blue squares, from the multi-configurational time-dependent Hartree (MCTDH) approach on the XCZ PES[19] as the red curve, and from MCTDH on the WWM PES[17] as the green curve.

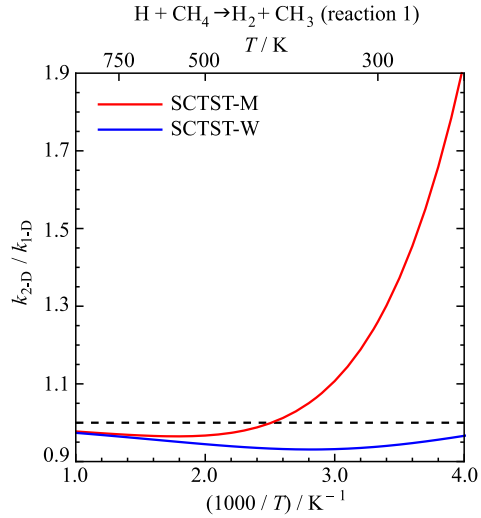

FIG. 4. Ratios of rate constants calculated within the 2-D framework to those calculated within the 1-D framework using the SCTST-M (red curve) and SCTST-W (blue curve) methods for reaction (1). The horizontal dashed line represents the value 1, at which 1-D and 2-D rate constants are equal.

III. RESULTS

A. Energetic parameters

The energetic parameters used in SCTST calculations are presented in Table I. The frequencies calculated from the PESs for reactions (1), (3), and (4) are equal to those from our previous work,[80] even though they were calculated in Jacobi coordinates. Detailed discussions of comparisons between these frequencies and those calculated by *ab initio* methods can be found in Ref. 80.

The anharmonic constants involving the transition mode (x_{1F} and x_{11}) are both zero in the one-dimensional case (Sec. II B 2). The anharmonic constant for the reaction mode in the two-dimensional case (x_{FF}) is considerably different from that in the one-dimensional case primarily due to the third term in Eq. (8a), which is not present in Eq. (9). For reaction (1), the absolute value of this term constitutes 49% of the 2-D x_{FF} parameter, and because it is negative, the magnitude of the 1-D x_{FF} parameter is 49% greater than the 2-D parameter. For reactions (2)–(4), the 1-D x_{FF} parameters differ from their 2-D counterparts by factors of 1.53, 2.12, and 1.58, respectively.

Notably, the magnitude of the 2-D x_{1F} parameter for reaction (4) is considerably less than those for reactions (1)–(3). Differences between 1-D and 2-D values of G_0 were considerably greater for reactions (1)–(3) than for reaction (4). The forward and reverse barrier heights of reaction (4) are equal due to the symmetry of this reaction.

B. H atom abstraction reactions

1. $H + CH_4 \longrightarrow H_2 + CH_3$ (reaction (1))

Rate constants for reaction (1) calculated using the 1-D and 2-D SCTST-M methods, QRS, and TST are presented in

TABLE II. Rate constants for reaction (1), in units cm^3 molecule^{-1} s^{-1}, calculated by TST, by the semiclassical methods discussed in this study, and by QRS.[a]

T (K)	TST	2-D SCTST-M	1-D SCTST-M	2-D SCTST-W	1-D SCTST-W	QRS[b]
200	8.52(−26)	4.57(−21)	9.07(−22)	3.03(−21)	2.97(−21)	5.67(−22)
250	8.26(−23)	5.77(−20)	2.99(−20)	4.85(−20)	5.02(−20)	1.53(−20)
300	8.25(−21)	5.84(−19)	4.64(−19)	5.46(−19)	5.82(−19)	2.33(−19)
350	2.26(−19)	4.55(−18)	4.27(−18)	4.42(−18)	4.75(−18)	2.25(−18)
400	2.77(−18)	2.65(−17)	2.65(−17)	2.61(−17)	2.80(−17)	1.50(−17)
450	1.98(−17)	1.18(−16)	1.21(−16)	1.17(−16)	1.25(−16)	7.34(−17)
500	9.73(−17)	4.20(−16)	4.34(−16)	4.19(−16)	4.43(−16)	2.80(−16)
600	1.11(−15)	3.20(−15)	3.32(−15)	3.21(−15)	3.36(−15)	2.34(−15)
700	6.57(−15)	1.51(−14)	1.56(−14)	1.52(−14)	1.58(−14)	1.16(−14)
800	2.59(−14)	5.17(−14)	5.32(−14)	5.19(−14)	5.37(−14)	4.07(−14)
1000	1.90(−13)	3.24(−13)	3.31(−13)	3.25(−13)	3.34(−13)	2.57(−13)
1300	1.34(−12)	2.05(−12)	2.09(−12)	2.06(−12)	2.10(−12)	1.57(−12)
1600	4.92(−12)	7.22(−12)	7.32(−12)	7.26(−12)	7.38(−12)	5.24(−12)
2000	1.65(−11)	2.36(−11)	2.38(−11)	2.37(−11)	2.40(−11)	1.57(−11)

[a]Numbers in parentheses denote powers of 10.
[b]From Ref. 77.

Figs. 2(a) and 2(b). The 1-D and 2-D SCTST-M results exhibit good agreement with each other over the temperature range in Fig. 2(a), differing at most by a factor of 1.93 at 250 K. Both of these rate constants also exhibit good agreement with QRS results over the temperature range considered in this study. At 250 K, the 2-D SCTST-M rate constant is 3.77 times greater than the QRS rate constant and 698 times greater than the TST rate constant. The 2-D SCTST-M rate constant is presented with results from full-dimensional theoretical studies in Fig. 3, although it is important to emphasize that these results were calculated on PESs constructed at a different level of theory and with a different dimensionality than the one considered in this study.

In order to gain insight into the factors that give rise to the difference between rate constants calculated using the 2-D and 1-D SCTST-M methods, we performed additional calculations in which some of the parameters used to calculate the CRP (x_{FF}, x_{1F}, x_{11}, and G_0) were varied individually. In each of these calculations, one of these parameters was assigned its value from the 1-D framework, and the remaining parameters

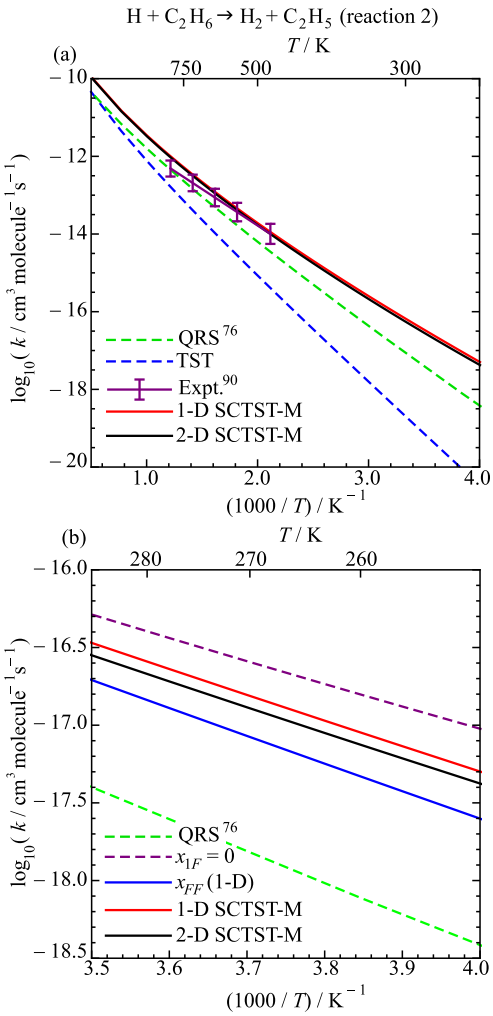

FIG. 5. (a) Rate constants for reaction (2) calculated using TST (dashed red curve), 2-D SCTST-M (black curve), and 1-D SCTST-M (blue curve) with QRS results from Kerkeni and Clary[76] (dashed green curve) and experimental results.[90] (b) Rate constants from additional calculations in which individual parameters (x_{1F}, magenta curve; x_{FF}, orange curve) were assigned values from a 1-D calculation.

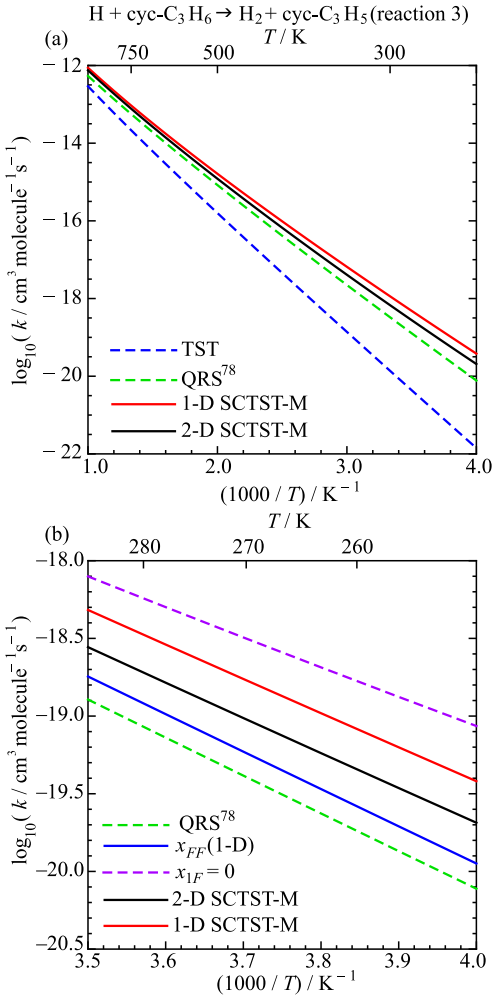

FIG. 6. (a) Rate constants for reaction (3) calculated by the 2-D (black curve) and 1-D SCTST-M (blue curve) methods, by TST (dashed red curve), and by QRS (dashed green curve) as reported by Shan and Clary.[78] (b) Results from additional rate constant calculations in which individual parameters were assigned their 1-D values (x_{1F}, magenta curve; x_{FF}, orange curve).

were assigned their values from the 2-D framework. Varying these parameters in this way enabled us to systematically evaluate which contribute most to the difference in results between the 1-D and 2-D methods. Figure 2(b) presents results from this analysis over a temperature range smaller than that in Fig. 2(a).

Assigning the parameter x_{1F} its 1-D value (0) causes the rate constant to increase relative to the 2-D case (by a factor of 2.42 at 250 K). This increase can be understood by considering the symmetric Eckart potentials that correspond to these calculations (Sec. II B 5), which are presented in Fig. 2(c) for $n = 0$. Because $\mathrm{Im}(x_{1F}) < 0$ for reaction (1), setting it to zero causes Ω_0 to increase (Eq. (23)). Ω_0 represents an effective reaction mode frequency, so an increase in this parameter causes a narrowing of the barrier. Narrowing the barrier decreases the barrier penetration integral and therefore increases the CRP and the rate constants. Only the $n = 0$ case is considered in this discussion because it contributes significantly more to the rate constant than the higher-energy $n = 1$ case due to the presence of a Boltzmann factor in Eq. (16).

TABLE III. Rate constants for reaction (2), in units cm^3 $molecule^{-1}$ s^{-1}, calculated by TST, SCTST, and QRS.[a]

T (K)	TST	2-D SCTST-M	1-D SCTST-M	2-D SCTST-W	1-D SCTST-W	QRS[b]
200	7.97(−24)	1.21(−19)	1.35(−19)	1.36(−19)	2.32(−19)	4.08(−21)
260	8.78(−21)	7.49(−18)	8.98(−18)	7.91(−18)	1.17(−17)	7.74(−19)
320	7.31(−19)	1.25(−16)	1.49(−16)	1.29(−16)	1.73(−16)	2.36(−17)
360	6.28(−18)	5.27(−16)	6.19(−16)	5.39(−16)	6.89(−16)	1.27(−16)
420	7.55(−17)	2.94(−15)	3.38(−15)	2.99(−15)	3.63(−15)	9.08(−16)
480	5.01(−16)	1.13(−14)	1.28(−14)	1.15(−14)	1.35(−14)	4.11(−15)
520	1.41(−15)	2.41(−14)	2.69(−14)	2.45(−14)	2.82(−14)	9.43(−15)
680	2.81(−14)	2.30(−13)	2.49(−13)	2.33(−13)	2.58(−13)	1.06(−13)
880	2.88(−13)	1.44(−12)	1.53(−12)	1.46(−12)	1.58(−12)	7.12(−13)
1000	7.78(−13)	3.24(−12)	3.42(−12)	3.29(−12)	3.51(−12)	1.61(−12)
1300	4.57(−12)	1.42(−11)	1.49(−11)	1.44(−11)	1.52(−11)	6.92(−12)
2000	4.55(−11)	1.05(−10)	1.09(−10)	1.06(−10)	1.11(−10)	4.50(−11)

[a]Numbers in parentheses denote powers of 10.
[b]From Ref. 76.

In contrast, assigning the parameter x_{FF} its 1-D value causes the rate constant to decrease relative to the 2-D rate constant (by a factor of 3.74 at 250 K). The reaction barrier in this case is wider than the 2-D barrier, and its asymptotes are greater due to a lesser value of D_{se} (Eqs. (25) and (27)). This results in less tunneling and a lower rate constant.

Assigning the parameter x_{11} its 1-D value (0) affected the rate constant negligibly, indicating that the transition mode for reaction (1) is not significantly anharmonic. This is illustrated in Fig. 2(d) in which the ratio of the anharmonic partition function for the transition mode to the harmonic partition function is presented as a function of temperature. This ratio is close to 1 from 250 K to 1000 K. At 250 K, the temperature of greatest difference between these partition functions, the rate constant calculated assuming that x_{11} is 0 is 0.05% greater than the 2-D rate constant.

Assigning the parameter G_0 its 1-D value also affected the rate constant negligibly because G_0 contributes negligibly to $\Delta V_f^{\ddagger}$. The absolute value of G_0 is 1.3% of $\Delta V_f^{\ddagger}$ in the 2-D case. The rate constant calculated by assigning G_0 its 1-D value is 3.2% greater than the 2-D rate constant at 250 K.

Only the changes in the x_{FF} and x_{1F} parameters contribute significantly to the difference in value between the 1-D and 2-D rate constants. The net effect of changing the x_{FF}, x_{1F}, and G_0 parameters on the barrier shape is represented as the 1-D SCTST-M barrier in Fig. 2(c). Because assigning x_{FF} its 1-D value decreases the rate constant and setting x_{1F} to 0 increases the rate constant by approximately the same factor, and because the G_0 and x_{11} parameters do not contribute significantly to the 2-D rate constant, the 1-D and 2-D rate constants for reaction (1) do not differ significantly. 1-D and 2-D rate constants calculated with the SCTST-M method are presented in Table II along with results from TST and QRS.

Differences between 2-D SCTST-M and 2-D SCTST-W results for reaction (1) are negligible and have been discussed previously.[80] The SCTST-W method is even less sensitive than SCTST-M to a reduction in dimensionality from 2-D to 1-D. At 250 K, the 2-D SCTST-W rate constant is 1.02 times greater than the 1-D SCTST-W rate constant. Ratios of the 2-D to 1-D rate constants for the SCTST-M and SCTST-W methods are presented in Fig. 4. Numerical values of rate constants calculated using 1-D and 2-D SCTST-W are also presented in Table II. The relative insensitivity of the SCTST-W method to a reduction in dimensionality will be discussed further in Sec. III C.

TABLE IV. Rate constants for reaction (3), in units cm^3 $molecule^{-1}$ s^{-1}, calculated by TST, SCTST, and QRS.[a]

T (K)	TST	2-D SCTST-M	1-D SCTST-M	2-D SCTST-W	1-D SCTST-W	QRS[b]
360	6.49(−19)	1.39(−17)	2.15(−17)	1.45(−17)	2.59(−17)	8.08(−18)
390	2.90(−18)	4.62(−17)	6.84(−17)	4.77(−17)	7.97(−17)	2.83(−17)
420	1.05(−17)	1.31(−16)	1.88(−16)	1.35(−16)	2.13(−16)	8.38(−17)
450	3.24(−17)	3.28(−16)	4.57(−16)	3.36(−16)	5.10(−16)	2.17(−16)
480	8.73(−17)	7.42(−16)	1.01(−15)	7.58(−16)	1.11(−15)	5.02(−16)
510	2.10(−16)	1.54(−15)	2.04(−15)	1.57(−15)	2.22(−15)	1.06(−15)
540	4.63(−16)	2.96(−15)	3.87(−15)	3.02(−15)	4.17(−15)	2.08(−15)
630	3.21(−15)	1.51(−14)	1.89(−14)	1.54(−14)	2.01(−14)	1.09(−14)
660	5.49(−15)	2.39(−14)	2.96(−14)	2.43(−14)	3.12(−14)	1.73(−14)
690	8.99(−15)	3.64(−14)	4.46(−14)	3.70(−14)	4.69(−14)	2.64(−14)
720	1.42(−14)	5.38(−14)	6.54(−14)	5.47(−14)	6.86(−14)	3.91(−14)
750	2.16(−14)	7.73(−14)	9.32(−14)	7.86(−14)	9.76(−14)	5.63(−14)

[a]Numbers in parentheses denote powers of 10.
[b]From Ref. 78.

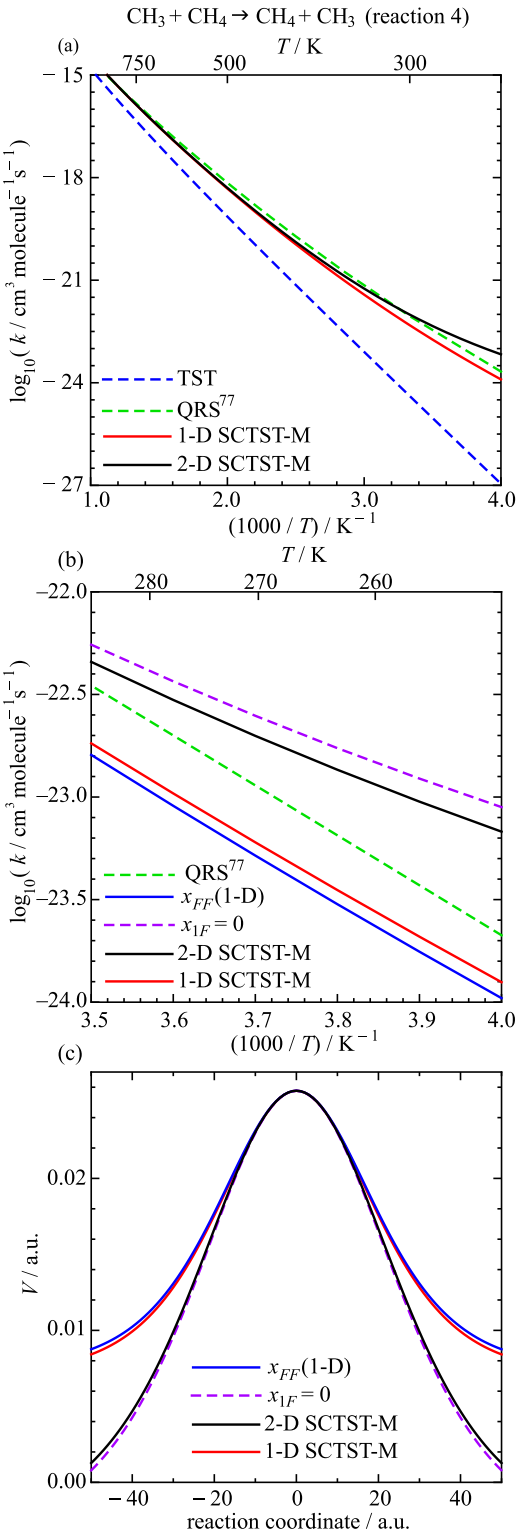

FIG. 7. (a) Rate constants for reaction (4) calculated by 2-D SCTST-M (black curve), 1-D SCTST-M (blue curve), QRS[77] (dashed green curve), and TST (dashed red curve). (b) Rate constants calculated by assigning the x_{1F} (magenta curve) and x_{FF} (orange curve) parameters their 1-D values individually. (c) Symmetric Eckart potentials for $n = 0$ corresponding to the SCTST-M results presented in (b).

2. $H + C_2H_6 \longrightarrow H_2 + C_2H_5$ (reaction (2)) and $H + cyc\text{-}C_3H_6 \longrightarrow H_2 + cyc\text{-}C_3H_5$ (reaction (3))

SCTST-M rate constants for reactions (2) and (3) are presented in Figs. 5(a) and 6(a) and Tables III and IV. As is the case for reaction (1), the 1-D and 2-D SCTST-M rate constants exhibit good agreement with each other from 250 K to 1000 K. At 250 K, 1-D rate constants are 1.19 and 1.85 times greater than 2-D rate constants for reactions (2) and (3), respectively. For reaction (3), 2-D rate constants also exhibit good agreement with QRS results,[78] differing by a factor of 2.66 at 260 K. For reaction (2), 2-D SCTST-M rate constants are greater than QRS results,[76] differing by a factor of 9.67 at 260 K, indicating that the SCTST-M method overestimates contributions from tunneling for this reaction.

This discrepancy can be attributed to a key difference between the SCTST methods and QRS. SCTST depends only upon the shape of the PES at the transition state, whereas QRS depends upon the shape of the PES from the interaction region near the transition state to the asymptotic region in the product and reactant channels. QRS is less sensitive than SCTST to the shape of the PES near the transition state. This suggests that further investigation of the accuracy of the PES for reaction (2) near the transition state is needed. The challenges involved in constructing an accurate PES are discussed in Ref. 89.

Figures 5(b) and 6(b) present rate constants calculated by varying each of the parameters x_{1F} and x_{FF} individually for reactions (2) and (3). As in reaction (1), $\mathrm{Im}(x_{1F}) < 0$ for both reactions, so assigning x_{1F} the value 0 resulted in a narrowing of their $n = 0$ potential barriers and therefore increased rate constants relative to the 2-D SCTST-M calculation (by factors of 2.25 and 4.19 at 250 K for reactions (2) and (3), respectively). It is interesting to note that the effect of the x_{1F} parameter on the rate constant is greater in reaction (3) than in reactions (1) and (2), primarily because the magnitude of x_{1F} is greater for reaction (3) than for reactions (1) and (2). This partially explains the fact that 1-D rate constants for reaction (3) are somewhat greater than 2-D rate constants, which was not observed in reaction (1), and which was observed to a lesser extent in reaction (2). Using the 1-D values of x_{FF} resulted in rate constants less than the 2-D SCTST-M rate constants by factors of 0.59 and 0.55 at 250 K for reactions (2) and (3), respectively.

As is the case for reaction (1), setting the parameters x_{11} and G_0 to their 1-D values affects rate constants negligibly, indicating that the x_{1F} and x_{FF} parameters are primarily responsible for differences between the 1-D and 2-D rate constants. At 250 K, the rate constant calculated assuming that $x_{11} = 0$ is 2.1% greater than the 2-D SCTST-M rate constant for reaction (2) and 17% greater for reaction (3). Using values of G_0 from 1-D calculations increased rate constants for reactions (2) and (3) by 8.2% and 20%, respectively, at 250 K.

Results from 1-D and 2-D SCTST-W calculations for these reactions exhibited excellent agreement with 1-D and 2-D SCTST-M results (Tables III and IV), suggesting that applying deep tunneling corrections does not appreciably improve the accuracy of SCTST calculations for these reactions.

C. $CH_3 + CH_4 \longrightarrow CH_4 + CH_3$ (reaction (4))

Calculated rate constants for reaction (4) are presented in Fig. 7 and Table V. At 250 K, the 2-D SCTST-M rate constant is 3.20 times greater than the rate constant calculated by QRS

TABLE V. Rate constants for reaction (4), in units cm^3 $molecule^{-1}$ s^{-1}, calculated by TST, SCTST, and QRS.[a]

T (K)	TST	2-D SCTST-M	1-D SCTST-M	2-D SCTST-W	1-D SCTST-W	QRS[b]
200	1.68(−31)	5.70(−25)	1.31(−26)	2.46(−25)	8.09(−26)	1.83(−26)
250	1.11(−27)	6.78(−24)	1.25(−24)	4.94(−24)	2.49(−24)	2.12(−24)
300	4.08(−25)	9.83(−23)	4.81(−23)	8.88(−23)	6.16(−23)	8.90(−23)
350	2.88(−23)	1.31(−21)	9.55(−22)	1.27(−21)	1.05(−21)	1.74(−21)
400	7.24(−22)	1.30(−20)	1.11(−20)	1.29(−20)	1.16(−20)	1.91(−20)
450	9.20(−21)	9.33(−20)	8.56(−20)	9.29(−20)	8.76(−20)	1.36(−19)
500	7.23(−20)	5.00(−19)	4.75(−19)	4.99(−19)	4.81(−19)	7.02(−19)
600	1.71(−18)	7.34(−18)	7.17(−18)	7.35(−18)	7.23(−18)	9.30(−18)
700	1.76(−17)	5.72(−17)	5.65(−17)	5.74(−17)	5.68(−17)	6.51(−17)
800	1.07(−16)	2.92(−16)	2.89(−16)	2.92(−16)	2.91(−16)	2.99(−16)
1000	1.52(−15)	3.35(−15)	3.32(−15)	3.36(−15)	3.34(−15)	2.83(−15)
1300	2.15(−14)	4.02(−14)	3.98(−14)	4.03(−14)	4.01(−14)	2.65(−14)
1600	1.31(−13)	2.25(−13)	2.22(−13)	2.26(−13)	2.23(−13)	1.21(−13)
2000	7.23(−13)	1.17(−12)	1.15(−12)	1.18(−12)	1.16(−12)	5.11(−13)

[a]Numbers in parentheses denote powers of 10.
[b]From Ref. 77.

and 6085 times greater than the TST rate constant. The fact that the ratio of the 2-D SCTST-M rate constant to the TST rate constant is considerably greater for reaction (4) than for the other reactions considered in this study indicates the relative importance of quantum tunneling effects in reaction (4). The difference between rate constants calculated using the 2-D and 1-D SCTST-M methods is also considerably greater for reaction (4) than for the other reactions considered. The 2-D rate constant is 5.42 times greater than the 1-D rate constant at 250 K.

The contributions of the x_{11} and G_0 parameters to the difference between 1-D and 2-D rate constants are insignificant, as in the other reactions. The rate constant obtained by assigning x_{11} the value 0 is 0.003% greater than the 2-D rate constant at 250 K, and the rate constant obtained by assigning G_0 its 1-D value is 3.1% greater.

There are two factors that primarily account for this relatively large difference between 1-D and 2-D rate constants. First, the difference between the rate constant calculated assuming that $x_{1F} = 0$ and the 2-D rate constant is significantly less for reaction (4) than for reactions (1)–(3). At 250 K, the rate constant from the $x_{1F} = 0$ calculation is 1.32 times greater than the 2-D rate constant (Fig. 7(b)), whereas this ratio is 2.42, 2.31, and 4.29 for reactions (1)–(3), respectively. The absolute value of the x_{1F} parameter is significantly less for reaction (4) than for reactions (1)–(3) (Table I). Because $x_{1F} < 0$ in all cases, assigning it the value 0 results in a broadening of the potential barrier. Less broadening is observed for the $n = 0$ barrier for reaction (4) because x_{1F} is less negative (Fig. 7(c)). Second, the ratio of the rate constant calculated using the 1-D value of x_{FF} to the 2-D rate constant is also considerably less for reaction (4) than for the other reactions. At 250 K, this ratio is 0.15, whereas for reactions (1)–(3), it is 0.27, 0.61, and 0.55, respectively. In the 1-D calculation for reaction (4), assigning the value 0 to the x_{1F} parameter does not increase the rate constant (relative to the 2-D case) as much as for the other reactions, and assigning x_{FF} its 1-D value decreases the rate constant more than in the other reactions.

For reaction (4), including deep tunneling corrections in rate constant calculations (the SCTST-W method) yields less significant differences between 1-D and 2-D results than when using the SCTST-M method, which does not include these corrections. The ratios of 2-D to 1-D rate constants calculated

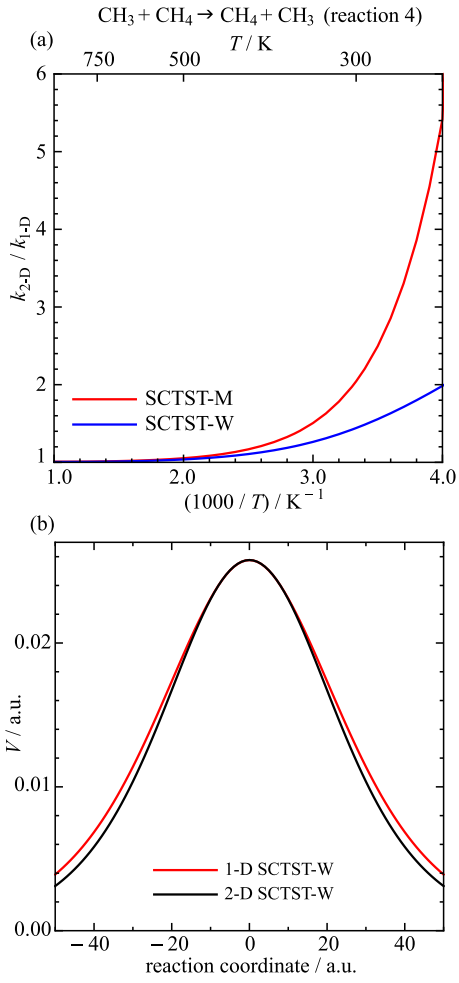

FIG. 8. (a) Ratios of 2-D rate constants to 1-D rate constants for reaction (4) calculated using the SCTST-M (red curve) and SCTST-W (blue curve) methods. (b) The potential barriers associated with the $n = 0$ case in SCTST-W calculations for reaction (4). The blue curve represents the barrier for the 1-D method, and the black curve for the 2-D method.

using the SCTST-M and SCTST-W methods are presented in Fig. 8(a). At 250 K, the 2-D SCTST-W rate constant is only 1.98 times greater than the 1-D SCTST-W rate constant, whereas the 2-D SCTST-M rate constant is 5.42 times greater.

This relative insensitivity of the SCTST-W method to a reduction in dimensionality can be understood by considering the potential barriers used in these calculations, which are presented in Fig. 8(b) for $n = 0$. The 1-D SCTST-W barrier (blue curve) is slightly greater than the 2-D barrier (black curve), but the difference between these barriers is only 0.0011 E_h at the point of greatest difference. In contrast, the difference between the 1-D and 2-D SCTST-M barriers for reaction (4) is significantly greater (Fig. 7(c)), tending to 0.011 E_h at the reactant and product asymptotes (Eq. (27)). Greater asymptotes result in less tunneling and therefore lower rate constants. Applying the SCTST-W method ensures that the barriers' asymptotes tend to physically realistic values, thereby eliminating the unrealistic differences between the asymptotes of the 1-D and 2-D barriers observed in the SCTST-M method. The SCTST-W method is therefore less sensitive to changes in the x_{FF} and x_{1F} parameters associated with reducing the dimensionality of the calculation from 2-D to 1-D, as these parameters determine the asymptotes in SCTST-M calculations.

IV. CONCLUSIONS

We applied one- and two-dimensional SCTST to calculate rate constants for four reactions involving the abstraction or exchange of an H atom. The frequencies, barrier heights, and 1-D and 2-D anharmonic constants used in these calculations were obtained from 2-D PESs developed previously by others for QRS calculations. We presented a novel method for calculating frequencies and anharmonic constants in Jacobi coordinates, which is more computationally efficient than previous methods and does not rely upon the assumption of a collinear geometry at the transition state. We also investigated the impact of the deep tunneling corrections to SCTST proposed by Wagner in the 1-D framework.

For the $H + CH_4$, $H + \text{cyc-}C_3H_6$, and $CH_3 + CH_4$ reactions, rate constants calculated by 2-D SCTST without deep tunneling corrections exhibit close agreement with QRS results, and for the $H + C_2H_6$ reaction, agreement is acceptable. For the $H + CH_4$, $H + C_2H_6$, and $H + \text{cyc-}C_3H_6$ reactions, 1-D rate constants calculated without deep tunneling corrections deviate little from 2-D results primarily due to two opposing effects approximately equal in magnitude. Assigning the anharmonic constants x_{1F} and x_{FF} their 1-D values results in increased and decreased rate constants, respectively, relative to the 2-D case. For the $CH_3 + CH_4$ reaction, assigning x_{1F} its 1-D value does not increase rate constants to the same extent as for the other reactions, so 1-D rate constants for this reaction are considerably less than 2-D rate constants. However, applying deep tunneling corrections rectifies this issue because it imposes more realistic behavior of the reactant and product asymptotes of the reaction barrier. It is particularly notable that a 1-D method yields rate constants in agreement with QRS results for this heavy–light–heavy reaction.

For the reactions considered in this study, we have demonstrated that treating only one DOF in SCTST calculations yields results that agree with 2-D QRS results calculated from the same PES, provided that deep tunneling corrections are applied. This suggests that SCTST can yield accurate reaction rate constants in a reduced-dimensionality framework and that the SCTST-W method should be applied in the 1-D framework, particularly given that its efficiency is comparable to SCTST-M. The primary cost of an SCTST calculation lies in the cost of constructing the requisite PES or calculating the potential directly by *ab initio* methods. Thus, reducing the number of dimensions treated explicitly in an SCTST calculation can significantly improve its efficiency via a need for a smaller region of the PES. In this study, we used analytical PESs that had already been developed, so 1-D calculations were not substantially faster than 2-D calculations. This suggests future investigation of the accuracy and efficiency of an *ab initio* RD SCTST approach.

ACKNOWLEDGMENTS

X. Shan and D. C. Clary acknowledge financial support from the Leverhulme Trust (Project Grant No. RPG-2013-321). S. Greene acknowledges financial support from the Rhodes Trust through a Rhodes Scholarship for graduate study.

[1]W. Hu and G. C. Schatz, J. Chem. Phys. **125**, 132301 (2006).
[2]P. D. D. Monks, J. N. L. Connor, and S. C. Althorpe, J. Phys. Chem. A **110**, 741 (2006).
[3]S. C. Althorpe and D. C. Clary, Annu. Rev. Phys. Chem. **54**, 493 (2003).
[4]G. Nyman and H.-G. Yu, Rep. Prog. Phys. **63**, 1001 (2000).
[5]J. M. Bowman and G. C. Schatz, Annu. Rev. Phys. Chem. **46**, 169 (1995).
[6]W. H. Miller, Annu. Rev. Phys. Chem. **41**, 245 (1990).
[7]J. M. Bowman, G. Czako, and B. Fu, Phys. Chem. Chem. Phys. **13**, 8094 (2011).
[8]J. Espinosa-Garcia, M. Monge-Palacios, and J. C. Corchado, Adv. Phys. Chem. **2012**, 164752.
[9]H. B. Schlegel, J. Comput. Chem. **24**, 1514 (2003).
[10]J. M. Bowman, Theor. Chem. Acc. **108**, 125 (2002).
[11]F. Huarte-Larrañaga and U. Manthe, J. Chem. Phys. **113**, 5115 (2000).
[12]F. Huarte-Larrañaga and U. Manthe, J. Phys. Chem. A **105**, 2522 (2001).
[13]T. Wu, H.-J. Werner, and U. Manthe, Science **306**, 2227 (2004).
[14]T. Wu, H.-J. Werner, and U. Manthe, J. Chem. Phys. **124**, 164307 (2006).
[15]G. Nyman, R. van Harrevelt, and U. Manthe, J. Phys. Chem. A **111**, 10331 (2007).
[16]G. Schiffel and U. Manthe, J. Chem. Phys. **132**, 084103 (2010).
[17]R. Welsch and U. Manthe, J. Chem. Phys. **137**, 244106 (2012).
[18]R. Welsch and U. Manthe, J. Chem. Phys. **138**, 164118 (2013).
[19]R. Welsch and U. Manthe, J. Chem. Phys. **142**, 064309 (2015).
[20]N. Bulut, J. Castillo, P. G. Jambrina, J. Kłos, O. Roncero, F. J. Aoiz, and L. Bañares, J. Phys. Chem. A **119**, 11951 (2015).
[21]S. Goswami, T. R. Rao, S. Mahapatra, B. Bussery-Honvault, and P. Honvault, J. Phys. Chem. A **118**, 5915 (2014).
[22]A. Fernandez-Ramos, B. A. Ellingson, B. C. Garrett, and D. G. Truhlar, in *Reviews in Computational Chemistry*, edited by K. B. Lipkowitz and T. R. Cundari (John Wiley & Sons, Inc., 2007), Vol. 23, Chap. 3, pp. 125–232.
[23]B. C. Garrett and D. G. Truhlar, "Variational transition state theory," in *Theory and Applications of Computational Chemistry: The First Forty Years*, edited by C. E. Dykstra, G. Frenking, K. S. Kim, and G. E. Scuseria (Elsevier, Amsterdam, 2005), Chap. 5, pp. 67–87.
[24]D. G. Truhlar, A. D. Isaacson, and B. C. Garrett, "Generalized transition state theory," in *Theory of Chemical Reaction Dynamics*, edited by M. Baer (CRC Press, Boca Raton, FL, 1985), Vol. IV, Chap. 2, pp. 65–137.
[25]T. C. Allison and D. G. Truhlar, "Testing the accuracy of practical semi-classical methods: Variational transition state theory with optimized multidimensional tunneling," in *Modern Methods for Multidimensional Dynamics*

Computations in Chemistry, edited by D. L. Thompson (World Scientific, Singapore, 1998), pp. 618–712.
[26]D. J. Arseneau, D. G. Fleming, Y. Li, J. Li, Y. V. Suleimanov, and H. Guo, "Rate coefficient for the ^{4}Heμ + CH_4 reaction at 500 K: Comparison between theory and experiment," J. Phys. Chem. B (published online).
[27]Y. V. Suleimanov and J. Espinosa-Garcia, "Recrossing and tunneling in the kinetics study of the OH + CH_4 → H_2O + CH_3 reaction," J. Phys. Chem. B (published online).
[28]M. Ng, D. K. Mok, E. P. Lee, and J. M. Dyke, Mol. Phys. **113**, 1511 (2015).
[29]S. Gong, Q. Luo, and G. M. Wei, J. Phys. Chem. A **119**, 4746 (2015).
[30]E. Gonzalez-Lavado, J. C. Corchado, Y. V. Suleimanov, W. H. Green, and J. Espinosa-Garcia, J. Phys. Chem. A **118**, 3243 (2014).
[31]R. Meana-Pañeda, D. G. Truhlar, and A. Fernández-Ramos, J. Chem. Theory Comput. **6**, 3015 (2010).
[32]R. Meana-Pañeda, D. G. Truhlar, and A. Fernández-Ramos, J. Chem. Theory Comput. **6**, 6 (2010).
[33]T. V. Albu, J. C. Corchado, and D. G. Truhlar, J. Phys. Chem. A **105**, 8465 (2001).
[34]I. R. Craig and D. E. Manolopoulos, J. Chem. Phys. **122**, 084106 (2005).
[35]I. R. Craig and D. E. Manolopoulos, J. Chem. Phys. **123**, 034102 (2005).
[36]Q. Meng, J. Chen, and D. H. Zhang, J. Chem. Phys. **143**, 101102 (2015).
[37]Y. V. Suleimanov, R. Collepardo-Guevara, and D. E. Manolopoulos, J. Chem. Phys. **134**, 044131 (2011).
[38]S. Jang and G. A. Voth, J. Chem. Phys. **112**, 8747 (2000).
[39]E. Geva, Q. Shi, and G. A. Voth, J. Chem. Phys. **115**, 9209 (2001).
[40]I. Navrotskaya, Q. Shi, and E. Geva, Isr. J. Chem. **42**, 225 (2002).
[41]G. A. Voth, D. Chandler, and W. H. Miller, J. Chem. Phys. **91**, 7749 (1989).
[42]T. J. H. Hele and S. C. Althorpe, J. Chem. Phys. **138**, 084108 (2013).
[43]S. C. Althorpe and T. J. H. Hele, J. Chem. Phys. **139**, 084115 (2013).
[44]W. H. Miller, J. Chem. Phys. **62**, 1899 (1975).
[45]W. H. Miller, Faraday Discuss. Chem. Soc. **62**, 40 (1977).
[46]W. H. Miller, R. Hernandez, N. C. Handy, D. Jayatilaka, and A. Willetts, Chem. Phys. Lett. **172**, 62 (1990).
[47]D. J. Griffiths, *Introduction to Quantum Mechanics*, 2nd ed. (Pearson Education, Inc., Upper Saddle River, 2005).
[48]I. M. Mills, "Vibration-rotation structure in asymmetric- and symmetric-top molecules," in *Molecular Spectroscopy*, edited by K. N. R. W. Mathews (Academic Press, New York, 1972), pp. 115–140.
[49]V. Barone, J. Chem. Phys. **122**, 014108 (2005).
[50]R. Burcl, N. C. Handy, and S. Carter, Spectrochim. Acta, Part A **59**, 1881 (2003).
[51]J. Neugebauer and B. A. Hess, J. Chem. Phys. **118**, 7215 (2003).
[52]W. Schneider and W. Thiel, Chem. Phys. Lett. **157**, 367 (1989).
[53]R. Hernandez and W. H. Miller, Chem. Phys. Lett. **214**, 129 (1993).
[54]T. L. Nguyen and J. R. Barker, J. Phys. Chem. A **114**, 3718 (2010).
[55]M. J. Cohen, N. C. Handy, R. Hernandez, and W. H. Miller, Chem. Phys. Lett. **192**, 407 (1992).
[56]M. J. Cohen, A. Willetts, and N. C. Handy, Chem. Phys. Lett. **223**, 459 (1994).
[57]T. L. Nguyen, J. F. Stanton, and J. R. Barker, J. Phys. Chem. A **115**, 5118 (2011).
[58]J. R. Barker, T. L. Nguyen, and J. F. Stanton, J. Phys. Chem. A **116**, 6408 (2012).
[59]R. E. Weston, Jr., T. L. Nguyen, J. F. Stanton, and J. R. Barker, J. Phys. Chem. A **117**, 821 (2013).
[60]A. F. Wagner, J. Phys. Chem. A **117**, 13089 (2013).
[61]J. M. Bowman, "Reduced dimensionality theories of quantum reactive scattering," in *Advances in Chemical Physics*, edited by I. Prigogine and S. A. Rice (John Wiley & Sons, Inc., Hoboken, NJ, 1985), Vol. 61, pp. 115–167.
[62]R. B. Walker and E. F. Hayes, "Reactive scattering in the bending-corrected rotating linear model," in *The Theory of Chemical Reaction Dynamics*, NATO ASI Series Vol. 170, edited by D. C. Clary (Springer, Netherlands, 1986), pp. 105–133.
[63]J. M. Bowman, J. Phys. Chem. **95**, 4960 (1991).
[64]D. C. Clary, Science **279**, 1879 (1998).
[65]F. Aguillon and M. Sizun, J. Chem. Phys. **112**, 10179 (2000).
[66]H. Szichman, M. Gilibert, M. González, X. Giménez, and A. A. Navarro, J. Chem. Phys. **113**, 176 (2000).
[67]H. Szichman, M. Gilibert, M. González, X. Giménez, and A. Aguilar, J. Chem. Phys. **114**, 9882 (2001).
[68]G. Nyman and D. C. Clary, J. Chem. Phys. **101**, 5756 (1994).
[69]G. Nyman, Chem. Phys. Lett. **240**, 571 (1995).
[70]G. Nyman, D. C. Clary, and R. D. Levine, Chem. Phys. **191**, 223 (1995).
[71]G. Nyman, J. Chem. Phys. **104**, 6154 (1996).
[72]T. Takayanagi, J. Chem. Phys. **104**, 2237 (1996).
[73]D. C. Clary and J. Palma, J. Chem. Phys. **106**, 575 (1997).
[74]J.-L. Le Garrec, B. R. Rowe, J. L. Queffelec, J. B. A. Mitchell, and D. C. Clary, J. Chem. Phys. **107**, 1021 (1997).
[75]B. Kerkeni and D. C. Clary, J. Chem. Phys. **123**, 64305 (2005).
[76]B. Kerkeni and D. C. Clary, J. Chem. Phys. **121**, 6809 (2004).
[77]S. T. Banks, C. S. Tautermann, S. M. Remmert, and D. C. Clary, J. Chem. Phys. **131**, 044111 (2009).
[78]X. Shan and D. C. Clary, J. Phys. Chem. A **118**, 10134 (2014).
[79]B. Kerkeni and D. C. Clary, Phys. Chem. Chem. Phys. **8**, 917 (2006).
[80]S. M. Greene, X. Shan, and D. C. Clary, J. Phys. Chem. A **119**, 12015 (2015).
[81]B. Amaee, J. N. L. Connor, J. C. Whitehead, W. Jakubetz, and G. C. Schatz, Faraday Discuss. Chem. Soc. **84**, 387 (1987).
[82]P. G. Mezey, "From reaction path to reaction mechanism: Fundamental groups and symmetry rules," in *The Reaction Path in Chemistry: Current Approaches and Perspectives* (Springer Science and Business Media, Dordrecht, 1995), pp. 11–38.
[83]V. Benderskii, D. Makarov, and C. Wight, in *Chemical Dynamics at Low Temperatures*, Advances in Chemical Physics Vol. 88, edited by I. Prigogine and S. A. Rice (Wiley, New York, 1994).
[84]A. Fernández-Ramos, J. A. Miller, S. J. Klippenstein, and D. G. Truhlar, Chem. Rev. **106**, 4518 (2006).
[85]P. A. Arnold and B. K. Carpenter, Chem. Phys. Lett. **328**, 90 (2000).
[86]B. Kerkeni and D. C. Clary, J. Chem. Phys. **120**, 2308 (2004).
[87]Wolfram Research, Inc., "Mathematica," version 8.0, Champaign, IL, 2010.
[88]Z. Ahmed, Phys. Lett. A **157**, 1 (1991).
[89]H. F. von Horsten, S. T. Banks, and D. C. Clary, J. Chem. Phys. **135**, 094311 (2011).
[90]M. G. Bryukov, I. R. Slagle, and V. D. Knyazev, J. Phys. Chem. A **106**, 10532 (2002).